Hard and soft plastic resin embedding for single-cell element uptake investigations of marine-snow-associated microorganisms using nano-scale secondary ion mass spectrometry

Andreas Rogge ,*[1] Clara M. Flintrop,[1,2,3] Morten H. Iversen ,[1,2] Ian Salter,[1,4] Allison A. Fong,[1]
Angela Vogts,[5] Anya M. Waite [1,6]

[1]Alfred Wegener Institute Helmholtz Centre for Polar and Marine Research (AWI), Bremerhaven, Bremen, Germany
[2]Marum and University of Bremen, Bremen, Germany
[3]Max-Planck-Institute for Marine Microbiology, Bremen, Germany
[4]Faroe Marine Research Institute, Tórshavn, Faroe Islands
[5]Leibniz Institute for Baltic Sea Research Warnemünde (IOW), Rostock-Warnemünde, Mecklenburg-Vorpommern, Germany
[6]FB2 Biology/Chemistry, University of Bremen, Bremen, Germany

Abstract

Marine snow aggregates are microhabitats for diverse microbial communities with various active metabolic pathways. Rapid recycling and symbiotic transfer of nutrients within aggregates poses a significant challenge for accurately assessing aggregate-associated turnover rates. Although single-cell uptake measurements are well-established for free-living microorganisms, suitable methods for cells embedded in marine snow are currently lacking. Comparable cell-specific measurements within sinking pelagic aggregates would have the potential to address core questions regarding aggregate-associated fluxes. However, the capacity to perform microscale studies is limited by the difficulty of sampling and preserving the fragile aggregate structure. Furthermore, the application of nano-scale secondary ion mass spectrometry (NanoSIMS) to aggregates is complicated by technical requirements related to vacuum and ablation resistance. Here, we present a NanoSIMS-optimized method for fixation, embedding, and sectioning of marine snow. Stable isotope labeling of laboratory-generated aggregates enabled visualization of label incorporation into prokaryotic and eukaryotic cells embedded in the aggregate structure. The current method is also amenable to various staining procedures, including transparent exopolymer particles, Coomassie stainable particles, nucleic acids, and eukaryotic cytoplasm. We demonstrate the potential for using structural stains to generate three-dimensional (3D) models of marine snow and present a simplified calculation of porosity and fractal dimension. This multipurpose method enables combined investigations of 3D aggregate structure, spatial microbial distribution, and single-cell activity within individual aggregates and provides new possibilities for future studies on microbial interactions and elemental uptake within marine snow.

Marine aggregates play a crucial role in the sequestration of photosynthetically produced organic matter, moving carbon from the euphotic zone to the deep ocean, which has an important impact on the global carbon budget (Turner 2015). They range from small conglomerates of organisms to aggregates of several millimeters in diameter, which also includes marine snow (aggregates > 500 μm; Alldredge and Silver 1988). The primary components of marine snow are phytodetritus, discarded appendicularian houses, fecal pellets, and other detrital material which stick together due to a matrix of exuded polymeric substances, including transparent exopolymer particles (TEP) (Passow et al. 1994; Passow et al. 2001; Turner 2015). The latter are defined as discrete exopolymers that consist predominantly of surface-active acidic polysaccharides and that are stainable with Alcian Blue (Alldredge et al. 1993; Cisternas-Novoa et al. 2015). Early studies revealed the importance of non-TEP extracellular polymeric substances (Stoderegger and Herndl 1999; Waite et al. 2005), and proteinaceous Coomassie stainable particles (CSP) (Long and Azam 1996) for aggregate structure. The first marine snow microstructure investigations also confirmed

*Correspondence: andreas.rogge@awi.de

these findings and provided insights into organism distribution (Heissenberger et al. 1996a; Leppard et al. 1996).

Microorganisms within organic aggregates benefit from highly concentrated substrate conditions (Shanks and Trent 1979; Lyons and Dobbs 2012) which characterize them as microscale nutrient patches in an otherwise homogeneous water column. Microbial abundances can be 10^3–10^5-fold higher than in the surrounding water column (Waite et al. 2000) and are typically associated with comparatively high-metabolic activity (Lyons and Dobbs 2012). Direct measurements of primary and bacterial production (Gotschalk and Alldredge 1989; Turley and Stutt 2000) and extracellular enzymatic activity (Karner and Herndl 1992; Zoppini et al. 2005) typically display enhanced values on aggregates relative to the water column.

Genomic profiling has also revealed that phylogenetic diversity of microbial assemblages associated with aggregates can differ from free-living communities (DeLong et al. 1993; Rath et al. 1998; Fontanez et al. 2015). Additionally, phylogenetic analyses revealed the presence of microbial communities capable of performing rare pelagic nutrient cycling processes such as ammonification (Shanks and Trent 1979), nitrification (Phillips et al. 1999), or methane production by archaea (Marty 1993; Maarel et al. 1999). Early studies suggested the potential existence of sub- or anoxic microzones within aggregates (Gowing and Silver 1983; Paerl and Pinckney 1996), and more recent work has demonstrated sub- and anoxic metabolic processes, such as anammox (Woebken et al. 2007), sulfate reduction (Vojvoda et al. 2014), or even chemolithoautotrophy (Swan et al. 2011) within aggregates from oxic or suboxic environments.

Based on a size-resolved particle model, Bianchi et al. (2018) estimated very recently that the anaerobic niche in the world oceans is expanded by particle-associated microenvironments which increases the rates of denitrification and sulfate reduction in the water column massively. Direct quantification of those and other nutrient turnover rates associated with marine snow, however, is difficult because numerous aggregates are required to generate results above measurable threshold values. This in turn necessitates bulk measurements which can be challenging to interpret due to the heterogeneous nature of aggregates. Furthermore, there is potential overlap of opposing metabolic pathways that can result in cryptic elemental cycling within single aggregates, as recently observed for the pelagic sulfur cycle in the Peruvian OMZ (Canfield et al. 2010). Emerging techniques such as single-cell measurements using nanoscale secondary ion mass spectrometry (NanoSIMS), or other modern technologies requiring vacuum conditions like electron dispersive X-ray, are powerful tools with the potential to yield insights into aggregate-associated nutrient fluxes. However, microzone investigations on marine aggregates that combine single-cell visualization, uptake measurements, and porosity measurements pose a significant challenge. Notable difficulties include (1) the preservation and handling of fragile

marine snow to reduce material loss, (2) the possibility for specific structural staining processes with reduced sample loss and dye precipitation, (3) the preservation of the three-dimensional (3D) structure enabling structure reconstruction for calculations of porosity and 3D fractal dimension, (4) the suitability for stable isotope enrichment measurements using NanoSIMS analyses with minimal enrichment dilution, and finally (5) stable storage conditions to ensure effective analyses in the field and at shore-based laboratories.

Here, we present a multidisciplinary method synthesis to address the challenges stated above, resulting in a widely applicable approach for microscopic investigations of marine snow, uptake measurements employing NanoSIMS, and structure reconstruction to facilitate porosity calculations. The characteristics of the resulting specimen matrix, including vacuum stability and negligible nitrogen and sulfur content, provide great potential for NanoSIMS-based flux investigations of individual organisms within an aggregate. Moreover, a streamlined workflow for biological and structural fixation combined with stable storage enables effective analyses in the field or at shore-based laboratories. Our preliminary investigations, as well as the recent literature (McGlynn et al. 2015), indicate that the fixation and storage conditions optimized for NanoSIMS and structural staining are potentially compatible with taxonomic staining procedures, such as fluorescence in situ hybridization (FISH) or catalyzed reporter deposition in situ fluorescence hybridization (CARDFISH), but this aspect of the method requires further optimization beyond the scope of the present objectives (*see* Supporting Information Chapter 1). A complementary embedding approach based on cryogel embedding is described in the companion paper by Flintrop et al. (2018), which enables taxonomic identification using FISH. We provide direct comparison of the two approaches (*see* "Discussion" section).

Using the plastic resin embedding procedure and structural stains, we describe a simplified calculation to determine porosity and fractal dimension based on a 3D reconstruction model. We also provide an alternative embedding protocol for aggregates comprised of very dense and/or terrigenous material, which allows structure-preserving bright field investigations and NanoSIMS measurements. A detailed description of the current methods and proposed applications is provided, as well as a field test of the embedding and structural staining. Our preliminary application of this approach demonstrates its potential to address existing gaps in our knowledge concerning biogeochemical fluxes as anaerobic cycling and microbial ecology of marine snow.

Methods

The final method for embedding of marine snow into an acrylic or epoxy resin consists of eight major steps (see Flowchart in Fig. 1): (1) The inactivation of biological activity and aggregate fixation with formaldehyde solution with subsequent washing in sterile seawater. Fixed aggregates are
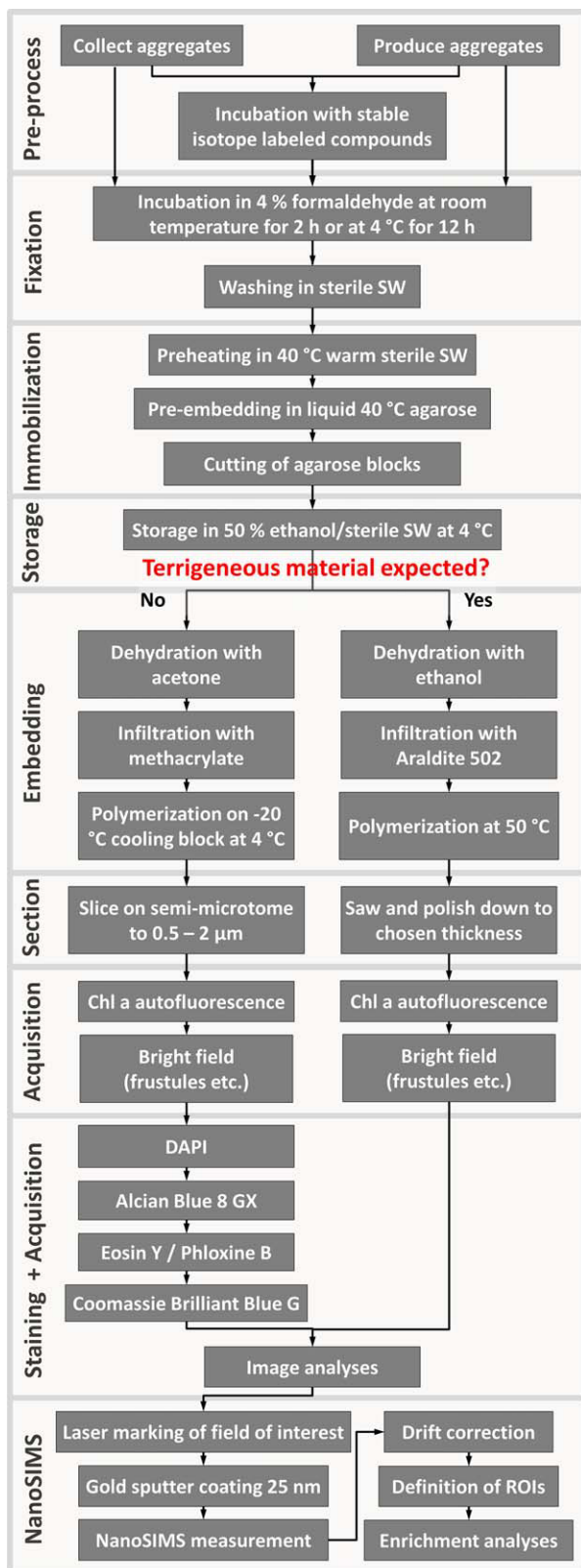
Fig. 1. Schematic outline of the presented method.

subsequently (2) immobilized and stabilized by pre-embedding in liquid agarose which can be followed by a storage step in ethanol solution. The stabilized aggregate is then (3) embedded in an acrylic or epoxy resin of choice, resulting in final structural and biological preservation, (4) sectioned and (5) stained using different structural, histological, and molecular dyes. Images of stained TEP, CSP, cytoplasm, and nucleic acid compounds as well as chlorophyll *a* (Chl *a*) auto-fluorescence are acquired and (6) structure is reconstructed in two or three dimensions, to allow porosity calculations. Finally, (7) embedded slices are prepared for NanoSIMS investigations, including laser-marking of the fields of interest, sputter coating, and fitting into the sample holder, followed by (8) NanoSIMS- and post-analysis.

In order to create a method suitable for structural staining and NanoSIMS analyses, we performed laboratory tests using a range of laboratory-generated aggregates, produced under controlled conditions (see details below). Mixed plankton communities were supplemented with natural marine bacterioplankton, and then incubated for 24 h with stable isotope-labeled glucose, nitrate, and sulfate (see below). We tested agarose as a pre-embedding matrix and the histological resin methacrylate as a final embedding medium. We applied several staining procedures, including Alcian Blue staining for TEP, Coomassie Blue staining for proteins, DAPI staining for nucleic acids, and eosin staining for eukaryotic cytoplasm proteins. The different structural signals were merged and a 3D model was created to illustrate the preserved structural features. NanoSIMS measurements were performed on one of the test aggregates to demonstrate the capacity to investigate single-cell element uptake employing the presented approach. To assess potential difficulties during the slicing process for aggregates with dense or terrigenous material, we also performed a test on dense aggregates, using agarose as a pre-embedding matrix and the resin Araldite 502 as a final embedding medium. This enables more precise sectioning for dense aggregates.

Generation of aggregates from laboratory phytoplankton cultures and surface water

Laboratory aggregates for methacrylate embeddings tests included a mixture of *Thalassiosira hyalina*, *T. marinoii*, *Emiliania huxleyi*, and *Micromonas pusilla* cultures in equal parts. This ensures applicability of the method for a diversity of aggregates by including soft as well as hard compounds, such as diatom frustules and coccoliths. Cultures were grown in F/2r medium (Guillard and Ryther 1962) with 12/12 h dark/light cycles for 7 d until the culture was opaque (cell numbers or growth phase not determined) before transfer of 1.8 L of culture mix into 2.1 L roller tanks. For bacterial colonization, 300 mL of 2 μm prefiltered North Seawater sampled in May off Bremerhaven (Germany) was added to the roller tanks (cell numbers not determined). The cultures were allowed to aggregate for 2 d at 2 rpm and 15°C in roller tanks in the dark.

In order to create very dense aggregates for alternative Araldite 502 embeddings, surface water sampled in March off Helgoland (Germany) was aggregated in roller tanks as described above for 4 weeks followed by direct fixation and embedding (*see* iii (b) "Methods" section) without prior incubation with stable isotope labeled compounds.

Stable isotope enrichment incubations

Aggregates containing stable-isotope-enriched organisms for NanoSIMS tests were formed by incubating laboratory generated aggregates in roller tanks with ^{13}C-labeled glucose, ^{15}N-labeled potassium nitrate, and ^{34}S-labeled sodium sulfate (see details below). Background concentrations of nitrate and sulfate in the sterile (0.2 μm filtered) North Seawater (sNSW) were measured prior to incubation using a QuAAtro39 Auto-Analyzer (Seal Analytical) to ensure correct labeling of ^{15}N and ^{34}S. All aggregate handlings and transfers were performed very gently, using either a bore pipette or a 1 mL pipette with cut pipette tips (*see* Table 1).

The lab aggregates were separated from free-living microorganisms by transferring each aggregate into a 50 mL centrifugation tube filled with sNSW. The aggregates were allowed to settle in the tube without reaching the bottom and then transferred into another tube with fresh sNSW, followed by transfer into a 50 mL roller tank. Triplicate 50 mL roller tanks, including 20–30 "washed" aggregates, were spiked with 10% $^{15}NO_3$ (Cambridge Isotope Laboratories, Cat.-No. NLM-765-PK) and 15% $^{34}SO_4$ (Sigma-Aldrich; Cat.-No. 718882) of the respective ambient concentration (12.47 μM NO_3, 25.44 mM SO_4), as well as 100 nM ^{13}C-glucose (D-glucose-$^{13}C_6$; Sigma-Aldrich; Cat.-No. 389374; background concentration not determined). Roller tanks were closed with a silicon stopper and rotated at 1.25 rpm and 15°C in the dark for 24 h before harvesting and embedding. To ascertain enrichment detection, triplicate controls were incubated with the same amount of unlabeled compounds and both groups analyzed to ensure an appropriate number of enriched aggregates for the analyses.

Aggregate embedding and analysis protocol

Biological fixation in formaldehyde solution and washing followed by immobilization in agarose is the first step in the procedure (Fig. 1). This step is the only step executed in the field. This prevents the risk of disaggregation during subsequent procedure and enables quick and easy sample handling during field campaigns as well as stable storage. The following dehydration, infiltration, and polymerization with resin enables thin sectioning of the aggregates in preparation for microscopy and SIMS analyses. A list of materials required is provided in Table 1.

i. Inactivation of biological activity and aggregate fixation

At the end of the 24 h aggregate incubation period, or immediately after aggregation in case of dense surface-water aggregates, aggregates were fixed in petri dishes filled with 0.2 μm-filtered 4% (v/v) formaldehyde/sNSW solution for 2 h at room temperature or at 4°C overnight (12 h). Stable isotope-labeled aggregates were subsequently washed in sNSW for 10 min and dense aggregates were washed for 30 min.

ii. Pre-embedding in liquid agarose and storage

Agarose solution was heated to boiling using a microwave. It was then kept at 40°C, along with the sNSW, in a hot water bath.

Following fixation, aggregates of both types were pre-heated by transferring them into 40°C warm sNSW for 10 min before transferring them into liquid, 40°C warm 6% (w/v) low-melting-point agarose (Omnipur® Agarose Low-Melting; EMD Chemicals) within silicon embedding molds. After cooling of the agarose at 4°C for 2 h, aggregates were cut out of the solid block using a sterile scalpel and forceps and transferred immediately into 2 mL centrifugation tubes filled with 0.2-μm-filtered 50% (v/v) ethanol/sNSW solution (molecular biology grade undenaturated absolute ethanol; Serva) to reduce biological degradation. Samples were stored at 4°C for 2 months.

iii. Embedding in acrylic resins

Final preservation was accomplished by embedding aggregates in an artificial resin resulting in solid, dehydrated, and sectionable blocks. Many resins for embedding were excluded prior to testing due to background fluorescence, polymerization temperatures above 60°C, or significant nitrogen and sulfur content rendering them unsuitable for potential rRNA-based hybridizations and NanoSIMS analyses, respectively. Moreover, hard materials such as sediments from terrigenous sources lead to rupture of the sections during the slicing process. Therefore, we tested the histology-originated methacrylate embedding medium for common "open ocean" aggregate samples which were sliced using a steel knife. We also tested the geology and soil sciences originated epoxy resin Araldite 502 which we sawed and polished to the desired thickness (40–140 μm).

(a) Methacrylate embedding for aggregates without terrigenous material

The methacrylate embedding protocol has been modified from the standard protocol (Velde et al. 1977). Dehydration was carried out in an increasing concentration series of acetone: Pre-embedded aggregates were transferred into snap cap vials and incubated twice with 50%, 70%, and 100% acetone on a tumbler for 1 h at room temperature. The methacrylate monomer was prepared by thoroughly mixing together 240 mL 2-hydroxyethyl methacrylate (Sigma Aldrich), 36 mL ethylene glycol butyl ether (Sigma Aldrich), and 0.81 g benzoyl peroxide (Luperox® A75; Sigma Aldrich). Infiltration started with a washing step with methacrylate monomer for 30 min followed by infiltration with monomer on a tumbler overnight at room temperature. Activator was

Table 1. List of required materials and instruments (n. d. = not determined).

Material	Company
Fixation	
Formaldehyde	Sigma Aldrich
sterile (0.2 μm filtered) seawater	n. d.
Petri dish	n. d.
Pre-embedding	
1 mL pipette	Eppendorf
Cut 1 mL pipette tips	Eppendorf
Bore pipette	n. d.
Agarose low-melting	Omnipur®; EMD chemicals
Sterile (0.2 μm filtered) seawater	n. d.
Embedding molds	n. d.
Microwave	Sharp
Water bath	Thermo Fisher Scientific
Scalpell	n. d.
Forceps	n. d.
50 mL centrifugation tubes	Sarstedt
Storage	
2 mL centrifuge tubes	Eppendorf
Ethanol (undenaturated for molecular biology)	Serva
Sterile (0.2 μm filtered) seawater	n. d.
Methacrylate embedding	
Forceps	n. d.
Scalpell	n. d.
Embedding molds	n. d.
Holder blocks	Custom made
Tumbler	Custom made
Refrigerator (4°C)	n. d.
Cooling blocks	n. d.
Snap cap vials	n. d.
Ultra-pure water	Millipore
Acetone	Sigma Aldrich
2-hydroxyethyl methacrylate	Sigma Aldrich
Ethylene glycol butyl ether	Sigma Aldrich
Benzoyl peroxide Luperox® A75	Sigma Aldrich
Polyethylene glycol 200	Sigma Aldrich
N,N-dimethylaniline	Sigma Aldrich
Methacrylate slicing	
Semi-automatic microtome	Leica
Humidity chamber	n. d.
Ultra-pure water	Millipore
Acetone	Sigma Aldrich
Biobond	EMS
Slides	Unimark
Heat plate	n. d.
Araldite 502 embedding	
Forceps	n. d.
Scalpell	n. d.
Embedding molds	n. d.
Tumbler	Custom made

TABLE 1. Continued

Material	Company
Snap cap vials	n. d.
Oven	n. d.
Ultra-pure water	Millipore
Ethanol (undenaturated for molecular biology)	Serva
Propylene oxide	Sigma Aldrich
Araldite 502 kit including DDSA and DMP-30	Electron microscopy sciences
Araldite 502 sectioning	
Grinding wheel	Wirtz
Carbid powder	Theodor Ehrich
Tap water	n. d.
Ethanol	n. d.
Körapox 439	Sikora
Stone saw Woco 50	Conrad
Grinding machine MPS 2 120	G&N
Grinding machine MPS 2 R 300	G&N
Aluminium oxide powder	Bühler
DAPI counterstaining	
Cover slips	Thermo Fisher Scientific
Ethanol for cleaning	Merck
4′,6-diamidino-2-phenylindole	Sigma Aldrich
Citifluor	Electron microscopy sciences
Vectashield	Vector laboratories
Ultra-pure water	Millipore
Sodium dodecyl sulfate	Merck
Alcian Blue staining	
Alcian Blue 8GX	Sigma Aldrich
Ultra-pure water	Millipore
Acetic acid	Merck
Ethanol (undenaturated for molecular biology)	Serva
Eosin staining	
Alcoholic eosin Y/phloxine B solution	Merck
Ultra-pure water	Millipore
Acetic acid	Merck
Coomassie Brilliant Blue staining	
Coomassie Brilliant Blue G	Sigma Aldrich
Ultra-pure water	Millipore
Ethanol (undenaturated for molecular biology)	Serva
Acetic acid	Merck

prepared by mixing 2 mL polyethylene glycol 200 (Sigma Aldrich) and 0.2 mL N,N-dimethyl aniline (Sigma Aldrich). All the infiltrated agarose blocks were carefully placed into individual embedding molds before 2 mL activator was added to 92 mL methacrylate monomer. The activated resin was added quickly into the molds, a holder block was placed on top of the molds and the embedding form was carefully

placed on a −20°C precooled cooling block and transferred into a 4°C refrigerator to avoid high temperatures during the exothermic reaction. After polymerization, resin blocks were cleaned of nonpolymerized resin using paper towel and were allowed to dry for several days at room temperature to finalize the hardening.

(b) Alternative Araldite 502 embedding for aggregates containing hard or terrigenous material

In order to embed dense aggregates, we used the Araldite 502 Kit (Electron Microscopy Sciences; Cat.-No. 13900). Embedding medium, consisting of 100 mL Araldite 502 (Sigma-Aldrich), 110 mL dodecenyl succinic anhydride (DDSA), and 4 mL 2,4,6-Tris(dimethylaminomethyl)phenol (DMP-30) was mixed thoroughly and stored at 4°C in sealed syringes until further processing.

Agarose blocks were dehydrated in snap-cap-vials on a tumbler, using an increasing concentration series of ethanol (molecular biology grade undenaturated absolute ethanol; Serva): 70% ethanol for 10 min, followed by two times 100% ethanol for 10 min. Afterward, ethanol was replaced by propylene oxide by incubating the blocks twice for 10 min in 100% propylene oxide, which enhanced the following infiltration with monomer.

Dehydrated agarose blocks were incubated in snap-cap-vials on a specimen rotator in an increasing concentration series of embedding medium and propylene oxide: starting with 25%, 50%, and finally 75% Araldite embedding medium in propylene oxide for 1 h, respectively. At last, agarose blocks were incubated in 100% embedding medium overnight (12 h) before transferring them into embedding molds and removing air bubbles in a desiccator under vacuum. Afterward, polymerization was carried out at 60°C for a minimum of 12 h.

i. Sectioning

To study the microscale 3D structure in aggregates of different densities, embeddings were sectioned using different approaches. Methacrylate embeddings were sliced on a semi-automatic microtome using steel knives, similar to the preparation of biological tissue samples, while Araldite 502 embeddings were sectioned by sawing and polishing; similar to petrographic thin sections.

In order to reconstruct the aggregate structure in three dimensions, we sectioned a 142 μm thick portion of one of our methacrylate embedded laboratory aggregate. To demonstrate the possibility for porosity and 3D fractal dimension estimation, we used 23 of the resulting 71 planes for the structural model.

(a) Sectioning of methacrylate embeddings

Methacrylate resin blocks were sliced with a thickness of 2 μm on a semi-automatic microtome (Leica) using a steel knife. Prior to slicing, resin blocks were placed in a humidity chamber (wet paper towel in closed plastic box) for at least 30 min to soften them and ease the slicing process. Slices

were placed on a drop of ultrapure water (UW; 18.2 Ω) on a clean glass slide (Unimark) followed by drying on a heat plate for 1 h (< 50°C).

(b) Sectioning of Araldite 502 embeddings

Alternative Araldite 502 embeddings were grinded and polished to different thicknesses down to 40 μm at the geology section of the University of Bremen. Samples were polished on a grinding wheel (Wirtz) using silicon carbid powder (Theodor Erich) and tap water until samples were level before they were cleaned with ethanol and adhered without air bubbles onto a transparent specimen holder using Körapox 439 resin (Sikora). Specimens were sawed using a Woco 50 stone saw (Conrad) to a thickness of 500–1000 μm before rough polishing down to the approximate thickness using a MPS 2 120 grinding machine (G&N). Finally, fine grinding to the final thickness of 40–140 μm and ultra-plane surface was done on a MPS 2 R 300 grinding machine (G&N) using aluminum oxide powder (Bühler).

ii. Structural and histological staining

To prevent overlapping of individual stains, staining and microscopy was performed in succession. After DAPI staining, DAPI signal and Chl *a* auto-fluorescence was acquired, followed by Alcian Blue staining and acquisition, eosin/phloxine staining and acquisition, and finally, Coomassie Blue staining and acquisition.

(a) DNA staining

Methacrylate slices were embedded with DAPI oil, consisting of 1% (v/v) 4′,6-diamidino-2-phenylindole (DAPI; Sigma-Aldrich) solution (100 μg mL^{-1}), 85% (v/v) Citifluor AF1 (Electron Microscopy Sciences) and 14% (v/v) Vectashield (Vector Laboratories), and closed with a cover slip (Thermo Fisher Scientific). After image acquisition (*see* vi in "Methods" section) of the DAPI and Chl *a* signal, the cover slip was removed very gently and DAPI-oil was washed off the specimen using 1% (v/v) sodium dodecyl sulfate solution for 15 min at room temperature followed by a washing step in UW for 10 min at room temperature and air drying.

(b) TEP staining

Alcian Blue, a polyvalent basic dye, was used to stain the TEP-fraction of aggregates. Alcian Blue stain solution consisted of 0.125% (w/v) Alcian Blue 8GX (Sigma Aldrich), 10% (v/v) acetic acid, 25% (v/v) ethanol, and 64.875% UW. Destain solution consisted of 25% ethanol, 10% acetic acid, and 65% UW. Sliced samples were incubated for 18 h in 0.2 μm filtered Alcian Blue stain solution at 4°C followed by a washing step in destain solution for 30 min to remove excess stain and to enhance contrast before 1 min of UW-washing and air drying.

(c) Cytoplasm staining

Cytoplasm structures, including proteins were stained with Eosin; a negatively charged acidic dye that stains basic and acidophilic structures. A mixture of eosin Y and phloxine B was used to enhance bright field signal intensity. Due

to the fluorescent properties of phloxine B, this combination of stains improved signal isolation during subsequent overlapping of images required for the structural model. Acetic acid was added to alcoholic eosin Y/phloxine B solution (Merck) to a final concentration of 0.25% (v/v). Samples were incubated at room temperature for 8 min in 0.2 μm filtered stain solution and subsequently washed in 0.25% (v/v) acetic acid in 90% ethanol/UW (v/v) for 30 min at room temperature to remove excess stain and to enhance contrast before 1 min of UW washing and air drying.

(d) Protein staining

Protein staining was accomplished by using the triphenylmethane dye Coomassie Brilliant Blue in an alcoholic and acetic solution. Coomassie Brilliant Blue solution consisted of 0.1% (w/v) Coomassie Brilliant Blue G 250 (Sigma Aldrich), 20% ethanol, and 3.75% acetic acid in UW. Slides were incubated in 0.2 μm filtered Coomassie Brilliant Blue solution for 1 h at 4°C, and washed for 30 min in 20% ethanol and 0.4% acetic acid at room temperature in UW to remove stain and enhance contrast. After a short washing step (1 min) in UW, the samples were air dried.

iii. Image acquisition, two-dimensional and three-dimensional reconstruction, and porosity calculation

Images were acquired on an Axioskop 2 plus epifluorescence microscope (Zeiss) equipped with a Ph1 Plan-Neofluar 10× objective and an Axiocam MRc5 camera (Zeiss) using Zeiss' Axiovision software. Alcian Blue, eosin Y/phloxine B, and Coomassie Blue images were acquired using bright field whereas DAPI, Chl *a* autofluorescence, and phloxine using the respective excitation and emission filter set. Using the software GIMP 2 (GNU Image Manipulation Program; Kimball et al. 1997–2017), images were contrast and brightness corrected. For overlap images, respective specific original channels (Coomassie and Alcian Blue, blue; DAPI, blue and cyan; Chl *a* autofluorescence as well as eosin/phloxine, red) were overlapped whereas residual channels were converted to the transparent alpha channel. For better visibility, colors were changed, i.e., when combining Alcian Blue and Coomassie Blue resulting in two blue channels (See figure descriptions). For the 3D model, aggregate positions of the individual planes were aligned manually (shift and rotation function) followed by aligning the dimensions (cut function). Construction of the 3D model was accomplished by importing all planes per channel as hyperstack into the Fiji-Bundle (Schindelin et al. 2012) of ImageJ (Schneider et al. 2012; Schindelin et al. 2015) using the importer of the Bioformats plugin (Linkert et al. 2010). The selected channel stacks were merged and the model calculated using the 3D-Viewer plugin (Schmid et al. 2010).

Porosity calculations were accomplished by merging all channels and thresholding the resulting stack with the optimal value to a binary stack. In every plane, the aggregate was defined manually by using the ROI-Manager tool (region of interest [ROI]) followed by interpolating those ROIs into three dimensions using the Interpolate ROIs tool of the ImageJ plugin BoneJ (Doube et al. 2010). Afterward, the percentage of pore volume to total aggregate volume inside the interpolated 3D-ROI was calculated using the surface mesh-based Volume Fraction function of BoneJ resulting in % of empty space or % porosity. The aggregate inside the interpolated 3D ROI (surface mesh) was visualized within the 3D-Viewer plugin of ImageJ.

Three-dimensional fractal dimension was calculated using the Fractal Dimension tool of BoneJ. The tool estimated the fractal dimension of the binary image stack by applying the box-counting algorithm as described for trabecular bone elsewhere (Fazzalari and Parkinson 1996). The program scanned boxes of diminishing size over the images and the number of boxes of each size containing foreground (aggregate) is counted. As the box size decreases, the proportion of boxes containing foreground increases in a fractal structure. The slope of the resulting linear function equals the fractal dimension.

iv. NanoSIMS preparations

Laser marking of spots of interest as well as bright field and DAPI image acquisition for later identification was carried out using a LMD7000 microscope (Leica) for labeled samples as well as controls. LMD-marked samples were cut to sample holder size using a glass cutter (Silberschnitt) and sputter coated with 25 nm gold using a 108 auto sputter coater (Cressington).

v. NanoSIMS measurements of single cells, image acquisition, and data processing

In order to measure single-cell uptake of stable-isotope-labeled glucose, nitrate, and sulfate, NanoSIMS imaging was performed using a NanoSIMS 50L instrument (Cameca, France) at the Leibniz-Institute for Baltic Sea Research Warnemünde (IOW). A $^{133}Cs^+$ primary ion beam was used to erode and ionize atoms of the sample surface. Six mass detectors equipped with electron multipliers (Hamamatsu) were used to record the received secondary ions $^{12}C^-$, $^{13}C^-$, $^{12}C^{14}N^-$, $^{12}C^{15}N^-$, $^{32}S^-$, and $^{34}S^-$ from the LMD-marked areas simultaneously. To suppress interferences, the mass resolving power was adjusted, allowing the separation of, e.g., $^{12}C^{15}N^-$ from interfering ions such as $^{13}C^{14}N^-$. Sample areas were sputtered for 1 min with 600 pA prior to analysis to reach the steady state of secondary ion formation. The primary ion beam current during the analysis was 2–3 pA; the scanning parameters were 512 × 512 px for areas of 20 × 20 μm to 60 × 60 μm, with a dwell time of 250 μs per pixel. Up to 120 planes were recorded.

The scans of each mass were accumulated and shift-corrected using the software Look@NanoSIMS (LANS; Polerecky et al. 2012). Cells were defined as ROI based on the $^{12}C^{14}N$ signal using the interactive threshold tool of the

same software. Isotope abundances for ^{13}C, ^{15}N, and ^{34}S were calculated and exported for each cell. Prokaryotic and algal cells were identified by shape using the DAPI, Chl *a*, and Bright Field image acquired prior to analysis.

Isotope abundances of individual ROIs of the labeled samples were corrected using the methacrylate resin as internal standard. The average stable isotope abundance of the resin of the unlabeled control measurements was subtracted from the stable isotope abundance of the resin of each measurement of each labeled sample. The resulting correction value was then added to each ROI of the respective measurement.

Enrichment threshold was defined for each type of heavy isotope as the maximum Poisson Error, calculated by LANS, of the unlabeled standard cells, respectively. Cells containing values greater than the threshold were defined as enriched. NanoSIMS images of the different isotope ratios were prepared as hue, saturation, and intensity (HSI) images using the software ImageJ and the plug-in OpenMIMS (Gormanns et al. 2012).

Field test using in situ collected marine snow

Aggregate samples were collected during the research cruise PS99 in July 2016 on board RV Polarstern west off Svalbard (78°58.85′N, 9°30.58′E) using a marine snow catcher (Osil, UK) with a volume of 100 L at 50 m depth. After recovery of the marine snow catcher, aggregates were allowed to settle down to the bottom chamber. The bottom chamber was then removed, and aggregates were harvested by hand using a 1 mL pipette with cut pipette tips. Fixation, storage, and methacrylate embedding as well as sectioning, DAPI, and TEP staining were performed as described in the main protocol above.

Assessment

The key challenges of microscale research on intact marine snow are (1) to reduce the loss of material, (2) ensure specific staining of structural compounds, (3) preserve the 3D structure to enable structure reconstruction for calculations of porosity and fractal dimension, (4) produce suitable samples for stable isotope enrichment measurements using nano-scale secondary ion mass spectrometer analyses with reduced enrichment dilution, and (5) to optimize the storage period to ensure effective analyses in the field and at shore-based laboratories. We tested how the method overcomes these challenges on laboratory-generated phytodetritus and also provide a (6) field test of the embedding principle by applying nucleic acid and TEP stain on methacrylate embedded marine snow sampled west off Svalbard.

Loss of material

While our method prevents loss of insoluble material during the washing and staining procedures that follow embedding, it is very difficult to estimate any loss of material during t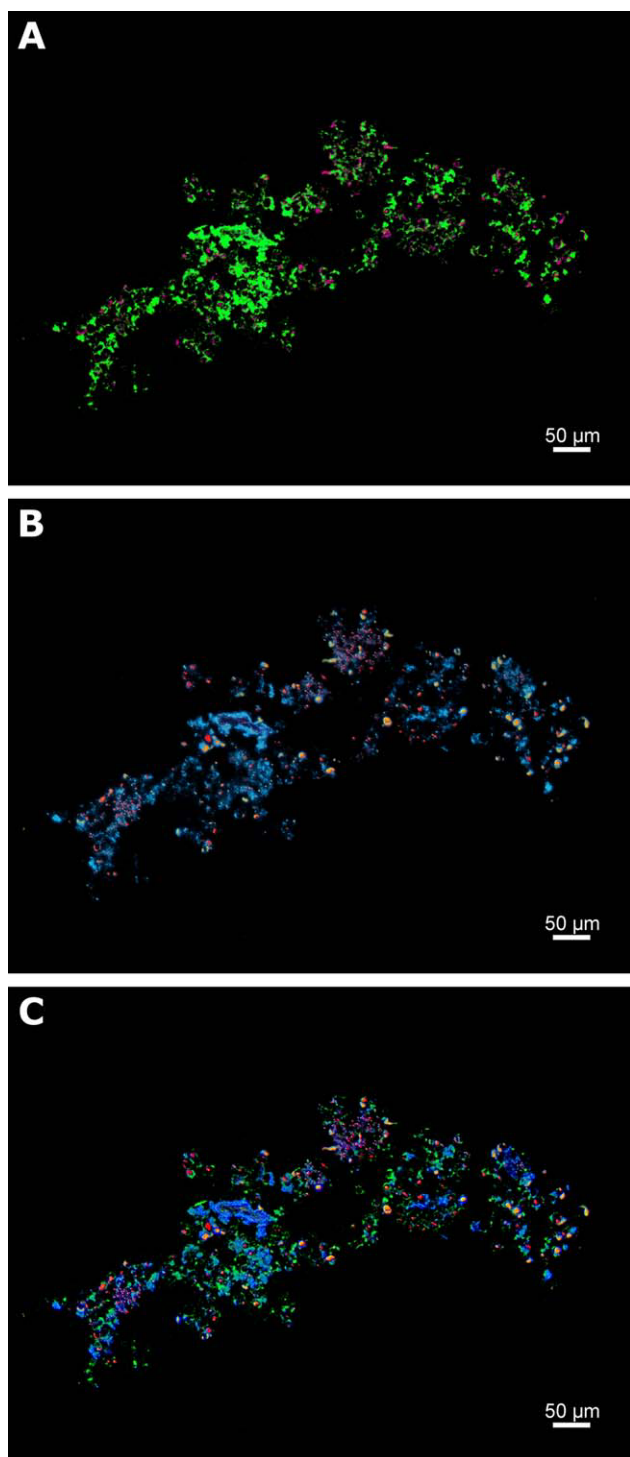he embedding process itself. Appropriate approaches to address material loss during handling are currently lacking. Considering the limited physical interaction with the aggregate surface following pre-embedding, it is reasonable to assume that the risk of losing insoluble material is limited to the period prior to completion of pre-embedding. Until this point, however, aggregates should be handled very carefully to reduce material loss and retain structural integrity during transfer. In particular, it is important to minimize the volume of water surrounding the aggregate to < 200 μL when it is transferred into agarose. Otherwise, dilution effects can result in soft pre-embeddings that perturb structure. Following these careful handling techniques, TEP structures and proteins remain undisturbed and are clearly arranged around algal cells (Fig. 2A,C, Supporting Information Fig. S1), demonstrating the procedure is capable of preserving aggregate structure.

It is also difficult to fully account for the loss of soluble material in water and the organic solvents (acetone or ethanol) used during resin embedding and the staining process. Nevertheless, we could clearly observe visible pigments in the chlorophyll auto-fluorescence signal (Fig. 2B), suggesting that pigments remain intact and can be used to visualize chloroplasts.

One possible limitation of our method is that the presence of very hard compounds, such as terrigenous material and diatom frustules, may lead to rupture of the specimen during the slicing process. We found that ensuring the use of newly sharpened knives on the microtome was able to prevent sample rupture in the presence of numerous diatom frustules. However, this is more problematic in the case of terrigenous material since the risk of damaging the microtome knife is very high. For aggregates of this nature, we recommend Araldite 502, instead of methacrylate, which is a more appropriate resin for hard embeddings (Fig. 3). Araldite 502 can be sawed and polished down to different section thicknesses. The equipment we had available when applying the Araldite 502 embedding procedure produced relatively thick sections (> 40 μm) that showed optimal characteristics for NanoSIMS as reported elsewhere (Herrmann et al. 2007; Mueller et al. 2012; Kaiser et al. 2015). However, structural staining was not applicable to Araldite 502 slices > 40 μm and it was only possible to prepare one slice per aggregate.

During the staining of methacrylate resin slices, detachment of the slice from the microscope slide may lead to the establishment of folds and sample loss. In order to address this limitation, we experimented with the use of adhesive coated slides (Biobond; Electron Microscopy Sciences), which proved successful for structural staining. However, also other adhesives, such as poly-L-lysine are widely used for this purpose (Huang et al. 1983; McGlynn et al. 2015). In our tests, also the use of a mixture of 2–10% acetone in UW as bedding between the slide and slice resulted in improved bonding characteristics that eliminated folding artifacts.

Fig. 3. Bright-field micrograph of an 80 μm thick slice through an Araldite 502 embedded aggregate formed from surface water off Helgoland, Germany. The resin did not allow structural staining, but valves and pigments are clearly visible. Araldite 502 sections are also amenable to NanoSIMS.

Fig. 2. Image overlap of the staining approaches. (**A**) Structural compounds TEP (green) and Coomassie stained proteins (magenta). (**B**) Distribution of nucleic acids stained with DAPI (blue), chlorophyll (red), and eukaryotic cytoplasm stained with eosin Y/phloxine B (yellow). (**C**) Overlap of all compounds mentioned above. Note that nucleic acid-rich areas without chlorophyll represent prokaryotes. Prokaryotes are distributed around algal cells and within a TEP matrix. Original images of each channel are provided in the Supporting Information Figs. S2–S7.

Stainability

The result of the different staining approaches for polysaccharides, proteins, cytoplasm, and nucleic acids are summarized in Fig. 2. Figure 2A exemplifies structural TEP and CSP staining, Fig. 2B shows organism distribution by visualizing nucleic acids, chlorophyll, and eosin, and Fig. 2C is an overlap of all channels. Examples for original images are provided in the Supporting Information Figs. S2–S7.

DAPI staining showed clear results that were distinguishable from background values, especially under higher magnification (Fig. 4). Prokaryotic cells were densely distributed around algal cells embedded within TEP-structures (Fig. 2B and Supporting Information Fig. S2). While the use of DAPI-oil is fast and convenient, we observed that even with anti-fading solution (Vectashield) bleaching of the dye occurred relatively quickly, by observation with UV-light ($\sim$ 5 min). An aqueous staining approach followed by embedding in anti-fading solution as reported for methacrylate embedded tissue might provide better results in cases where longer observation times are required (Bako et al. 2015).

Staining with Alcian Blue is a well-established method, which enables the visualization of negatively charged, sulfated, and carboxylated polysaccharides (Decho 1990) and was first reported for transparent exopolymeric particles by Alldredge et al. (1993). There are no reports of Alcian Blue staining of TEP-compounds with methacrylate embedded samples; however, we were able to achieve successful staining when applied in an ethanol solution. The stain is distinctly visible and the localization of TEP around algal cells follows the expectation that phytoplankton exudates would be present in aggregates (Fig. 2A, Supporting Information
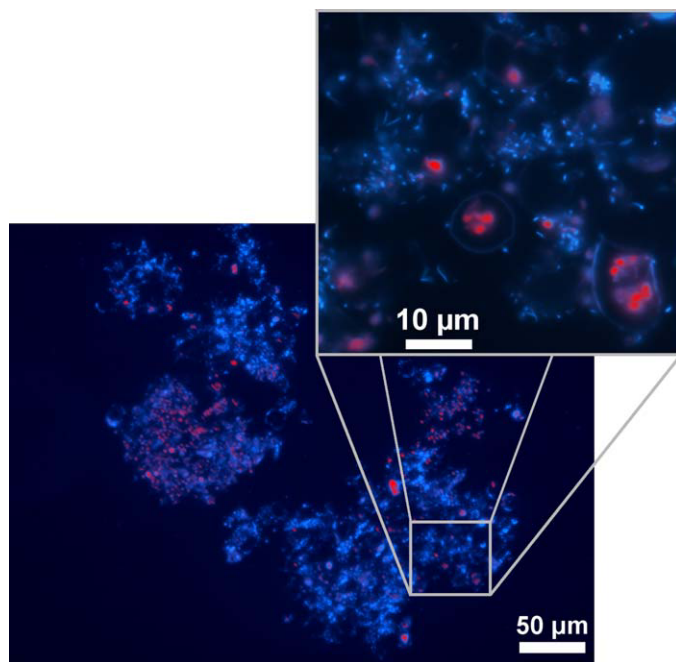
Fig. 4. Two micrometer thick slice of the methacrylate embedded aggregate used for NanoSIMS: The overlap of the DAPI stained nucleic acid channel in blue and the red Chl *a* autofluorescence channel enables the identification and distribution of prokaryotes and algae. Bigger cells with red compartments are chloroplast containing algae which are mostly surrounded by small prokaryotes without chlorophyll. The inset area represents area analyzed by NanoSIMS (*see* "Utility for stable isotope enrichment measurements" section). Note that cells and compartments that are not in focus are located in deeper slice layers and might not appear in the surface based NanoSIMS image.

Fig. S1). Importantly, dye coagulation or interference with salts which lead to overestimations of TEP signals as reported for staining in situ or on filters (Passow and Alldredge 1995; Cisternas-Novoa et al. 2015), can be excluded here. Since aggregate sections are still embedded within the resin during the staining process, it is possible to remove Alcian Blue particles by intense washing without risking sample loss.

Eosin, a halogenated derivative of fluorescein, binds to basic poly-amino acids, such as histidine, arginine, lysine, and tryptophan under acidic conditions (Waheed et al. 2000). It is a well-established and commonly used method to stain eukaryotic cytoplasm in histology (e.g., Veta et al. 2014), whereas mainly negatively charged bacterial cytoplasm may be stained with other dyes instead (Becerra et al. 2016). In combination with phloxine B, a chemically related compound to eosin Y, it is possible to increase bright-field intensity and enhance fluorescence signals (Carvalho and Taboga 1996; Aylon et al. 2016) (Fig. 2B, Supporting Information Figs. S5, S6). In our laboratory aggregates, the signal of eosin Y/phloxine B overlapped with chlorophyll, which is expected since eukaryotic organisms were the only cytoplasm containing cells stainable with eosin. This results in a

combined approach necessary for total cytoplasm visualization in future studies.

Coomassie Brilliant Blue, originally used to stain proteins in polyacrylamide gels (Fazekas et al. 1963), is a common dye for proteinaceous particles in the water column (Long and Azam 1996). We show that when applied in an alcoholic and acidified solution, it is also possible to stain methacrylate sections (Supporting Information Fig. S7). However, we only detected distinct CSP signals within internal algae structures (Fig. 2A), i.e., no external signals were visible. It is possible that since Coomassie Brilliant Blue staining was done after TEP staining the stains overlapped precluding the identification of CSP structures within the aggregate. Alternatively, the lack of areas with exclusive extracellular CSP labeling might also be explained by aggregate composition. Differences would be expected in aggregates with TEP-producing eukaryotic algae and microbes only, compared to different types of particles (CSP) produced by different species such as cyanobacteria at different growth phases (Cisternas-Novoa et al. 2015). However, due to the observation of stained protein-containing algal structures, CSP remains a possibility for staining in future studies. As reported for Alcian Blue staining above, an overestimation of CSP by dye precipitation can be excluded by intense washing of the specimen without sample loss.

Alternative Araldite 502 embeddings for dense aggregates were not stainable with any of the dyes tested above. However, observation of nontransparent compounds, such as frustules and pigments was possible (Fig. 3).

Three-dimensional aggregate structure

Two-dimensional visualizations enable investigations on organism distributions, including algae-bacteria associations or inter-cellular material distributions such as TEP or CSP (*see* Fig. 5C). However, structural investigations on porosity or fractal dimension require the implementation of the third dimension. Therefore, we demonstrate the reconstruction of a 3D structure using 23 of 71 planes of a 142 μm thick segment of a laboratory-generated aggregate (Fig. 5).

Using the plugin BoneJ, we calculated the number of voxels (volumetric pixels) filled by particulate material (merged channels of TEP, CSP, nucleic acid chlorophyll, and cytoplasm) and the total number of voxels. Definition of the aggregate boundary is difficult and controversial, and currently beyond the scope of this study. To illustrate the possibility of porosity calculation, using our embedding method, we defined the boundary manually as close as possible to the particulate material while including pores (*see* Fig. 5C). For future investigations, we recommend a standardized approach to define the boundary, such as by applying a modified script of the automatic ROI definition tool in ImageJ or elliptical approximations of the boundary using the estimated cross-sectional area as reported elsewhere (Dörgens et al. 2015; Flintrop et al. 2018). In this
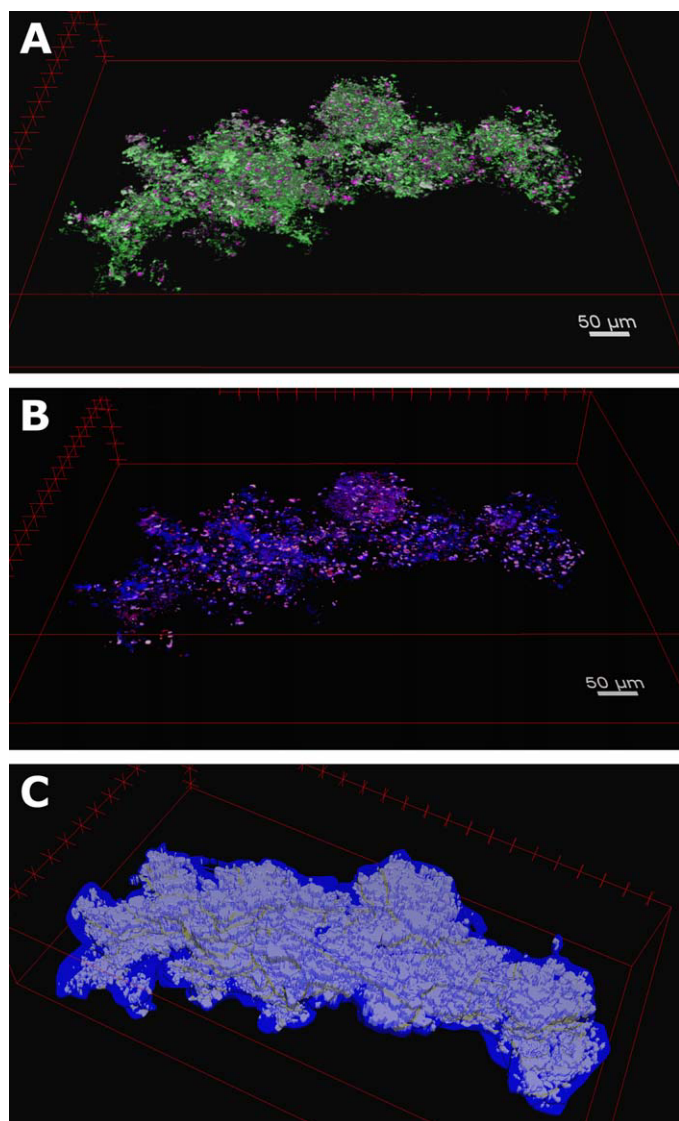
Fig. 5. Three-dimensional reconstruction of an aggregate segment. (**A**) Structural compounds TEP (green) and Coomassie Brilliant Blue stained proteins (magenta). (**B**) Nucleic acids (blue) and chlorophyll (red) as well as eukaryotic cytoplasm (yellow). (**C**) Visualization of the porosity calculation using BoneJ. All channels were merged and converted to a binary stack, whereas a 3D ROI (blue) defined the boundary of the aggregate.

demonstration, we used 23 of 71 planes, but we recommend using as many planes as possible to increase precision. We estimated a porosity of 66.5% in our test aggregate compartment. This is somewhat low compared to other calculations of phytodetritus aggregates (97–99.9%; Alldredge and Gotschalk 1988) and is closer to values reported for copepod fecal pellets (Ploug et al. 2008). Previous estimates of marine aggregate porosity are based on volume to dry weight ratios (Alldredge and Gotschalk 1988; Ploug et al. 2008). The approach employed here was based exclusively on volumetric ratios, i.e., the ratio of stained hydrated compounds to total aggregate volume. Water-containing compounds in bacteria or algae, as well as TEP or CSP may have higher volumes when hydrated leading to lower porosity estimates in our approach. This is of course a matter of definition, but when considering, that these values may be used in hydrodynamic models for aggregate and particle settling behavior, our approach might provide realistic results because water does not flow through enclosed water intrusions such as organisms, or hydrated matter as TEP or CSP. For the same aggregate portion, we also calculated a 3D fractal dimension of 2.13. Natural aggregates are characterized by fractal dimensions between 1 (tenuous and stringy) and 3 (dense and opaque) (Kranenburg 1994). The fractal dimension calculated in this approach is comparable to aggregates sampled at depths > 400 m (Risović 1998), when considering the likely differences that exists between laboratory-generated and natural aggregates.

Utility for stable isotope enrichment measurements

Methacrylate embedded samples investigated via Nano-SIMS were characterized by a plane surface and a stabilized structure under ultra-high vacuum conditions with no outgassing observed. This is also evident from comparisons of epifluorescence (Fig. 4) and secondary electron images of the same region (Fig. 6). The airlock reached full vacuum (3.7–8 mbar) in 60 h after loading three 2 μm thick methacrylate samples into the chamber. When the samples were loaded into the NanoSIMS analysis chamber, normal operation vacuum (2.5–10 mbar) was reached within 15 min. This behavior indicates negligible outgassing of methacrylate when applying a slice thickness of 2 μm. Several failures on the surface, such as scratches and holes could be observed in the secondary electron image (Fig. 6), which was likely due to slightly rough handling while placing the sample into the holder. Negative effects, such as ablation, however, were not observed.

Element uptake into single cells was successfully visualized and calculated based on NanoSIMS measurements of methacrylate embedded aggregates. We observed one ^{15}N and several ^{34}S enriched organisms in laboratory generated aggregates incubated with stable isotope tracer compounds occurring predominantly in prokaryotic cells (Figs. 7 and 8). The low number of ^{15}N enriched cells may, next to inactive cells, be explained by the use of alternative nitrogen sources such as ammonia. Moreover, the location of enzymes involved in prokaryotic nitrate reduction may prevent uptake: only assimilatory reductase enzymes (Nas) are located within the cytoplasm, whereas respiratory (Nar), and dissimilatory nitrate reductase (Nap) enzymes are membrane-bound or located in the periplasm, respectively (Moreno-Vivián et al. 1999). The latter enzyme leads to direct export of nitrate reduction products out of the cell after uptake inside the periplasm.
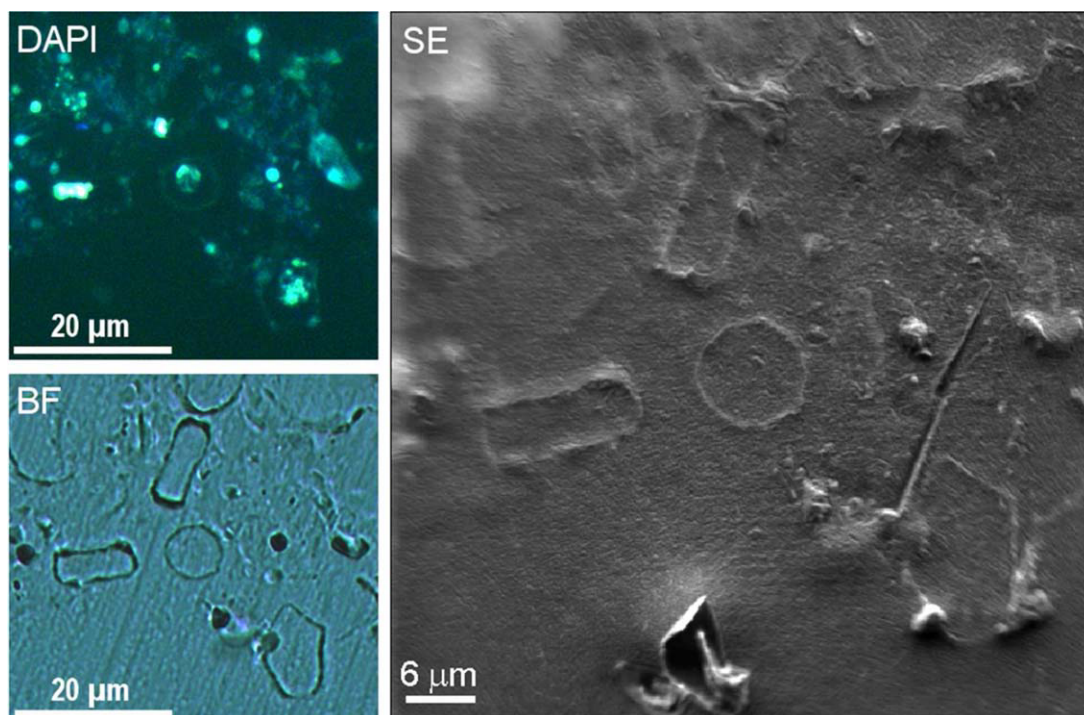
Fig. 6. Structural characteristics of methacrylate embeddings during the NanoSIMS measuring process: DAPI and bright field (BF) images were taken on a Laser Micro Dissection microscope (LMD7000, Leica) and the secondary electron image was acquired in the NanoSIMS 50L (Cameca). Structural differences caused by ultra-high vacuum as inflation, contraction, or detachment could not be observed compared to the sample structure at atmospheric pressure. Visible effects as the hole on the bottom or the scratch in the right middle were caused by sample treatment using forceps. Note that fluorescence differences to Fig. 4 are caused by removed DAPI stain and immersion oil prior to Laser marking.

Original abundance values of cells from ^{13}C incubations have on average an approximately 1‰ lower ^{13}C abundance compared to control incubations (Supporting Information Fig. S16). Higher Poisson errors associated with these cells indicate internal measurement effects as a likely explanation for this difference. These may include a different angle of the primary ion beam or slightly shifted detector positions on the mass peak of the respective isotopes due to the separation of measurements by several days. Based on the fact that all our methacrylate samples were embedded using the same batch of resin mixture at the same time, we were able to use an abundance correction approach based on resin abundances serving as internal standard. This calculation eliminates the internal measurement effects and enables correct result interpretation (Fig. 8 vs. Supporting Information Fig. S16). Taking these considerations into account, we might interpret a trend toward enrichment for a small number of ^{13}C-incubated cells as well. It is also probable that a matrix effect leads to dilution of the ^{13}C-signal in methacrylate resin embeddings. However, quantifying the dilution factor is challenging because of variable and unconstrained infiltration in different aggregates that is partly related to material density. This should be considered when combining quantitative measurements, as, e.g., total uptake measurements, with

qualitative NanoSIMS measurements of aggregates of different density. The background content of N and S in methacrylate resin is negligible, resulting in stronger signals and low dilution of ^{15}N and ^{34}S enrichments (Fig. 7). Secondary ion yields were comparable to previous applications, such as bacterial samples on gold sputtered polycarbonate filters (Rogge et al. 2017), signifying adequate ionization efficiencies in embedded samples.

The utility of Araldite 502 embeddings for ultra-high vacuum applications, such as NanoSIMS, has been demonstrated previously (Herrmann et al. 2007; Clode et al. 2009; Mueller et al. 2012; Kaiser et al. 2015). Key attributes include very low outgassing characteristics as well as structural stability without ablation. In this study, we did not specifically test its efficacy.

Storage life

In our tests, we started the final resin embedding 2 months after sampling when the agarose blocks were still intact. This time should be sufficient for sample storage during periods between most field collections and lab-based processing. We observed that 50% sterile seawater and storage above the freezing point prevents cell bursting and the presence of ethanol serves as biological preservative. Ethanol is also used as a rRNA preservative for FISH (Shiraishi et al.
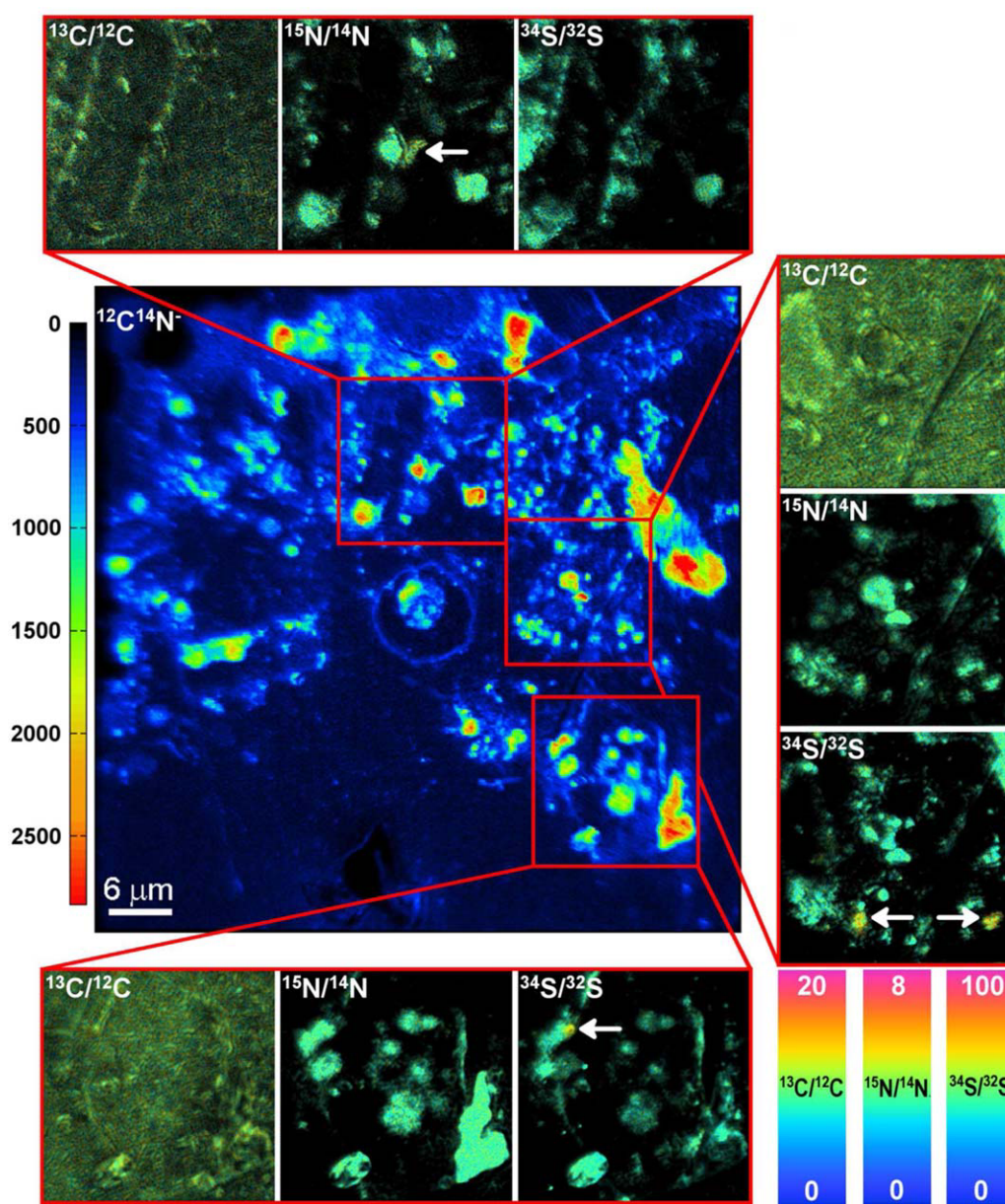
Fig. 7. Secondary ion mass spectrometry measurements on a 2 μm thick methacrylate embedded lab aggregate: The $^{12}C^{14}N^-$ signal as overview image was used to identify biomass and to locate spots for detailed ratio measurements. Significant and visible enrichments of ^{15}N could be detected in one prokaryotic cell in the upper spot while significant and visible enrichments of ^{34}S could be detected in the middle and lower spot. A low background in the N and S signal enables the precise definition of cells. Isotope ratios are presented as HSI-image enabling brightness adjusion of each pixel based on respective ion counts whereas black areas correspond to areas with low ion counts. The scales of isotope ratios are presented in per mill.

2008). We did not perform a time-course study of preservation properties of agarose-embedded and preserved aggregates, as it was secondary to the main issue of optimizing embedding techniques for NanoSIMS analyses. However, given previous findings using ethanol as a preservation solution for both nucleic acids and biofilm samples (Shiraishi et al. 2008), we are confident that biological components were stabilized.

Field test using in situ collected marine snow

To test aggregate handling and pre-embedding in more realistic conditions at sea, we performed aggregate sampling in Fram Strait close to the coast of Svalbard using a marine snow catcher. No difficulty in aggregate handling, leading to material loss due to disaggregation during transfer steps, could be observed. Even though the aggregates were relatively close to the coast and Kongsfjorden, the content of terrigenous material was low, so that slicing of methacrylate

Fig. 9. Overlap micrograph of marine snow sampled off Svalbard, Norway: DAPI stained nucleic acids (blue) and Chl *a* (red) as well as Alcian Blue stained TEP (green) in top image of a slice through the whole aggregate. The bottom image, showing a part of the aggregate in higher magnification, exemplifies nucleic acid staining (blue) and Chl *a* (red).

trip: samples were resin embedded approximately 3 months after sampling and pigment localization and concentration as well as the structure is still undisturbed.

Discussion

The microstructure of marine snow is likely to impact the scale and availability of diverse microbial niches within these particles. In turn, microbially mediated transformations of particulate matter can influence the regeneration of (sometimes limiting) nutrients and carbon-specific remineralization rates. These specific processes within marine snow may affect the efficiency of the biological carbon pump, pelagic-benthic coupling, and physical transport of microbial communities. Understanding the importance of these processes within aggregates is currently limited by a lack of suitable methods. To broaden our knowledge on microscale structures, microbial communities, and uptake rates associated with marine snow, we sought to develop a multipurpose method for the preservation and slicing of marine snow that was compatible with different structural stains and NanoSIMS investigations.

Several approaches for the investigation of marine snow have been developed during recent decades. To date, these have mainly focused on characterizing features on whole aggregates, such as Alcian Blue and Coomassie Blue staining on membrane filters for total exopolymer equivalents (Busch et al. 2017) or fingerprinting and sequencing techniques for aggregate-associated microbial community structure (DeLong et al. 1993; Rath et al. 1998; Fontanez et al. 2015). For such

Fig. 8. Isotope abundances in ‰ including Poisson Errors as error bars, of all measured prokaryotic and phytoplankton cells as well as the resin itself corrected by using the resin as internal standard. The dashed line indicates the enrichment threshold (maximum value of the Poisson error of controls). Respective ROIs are shown in Supporting Information Figs. S8–S15.

was successful. As shown in Fig. 9, chlorophyll and nucleic acid signals are distinct and TEP compounds are intensely stained. Also the storage time was adequate for this field

objectives, capturing particles and aggregates on membrane filters is sufficient. However, such sampling methods lead to loss of 3D structure and material and are not suitable for addressing the microscale structure of individual marine aggregates. The idea of slicing marine snow was developed for TEM investigations using the melamine resin Nanoplast® (Heissenberger et al. 1996b; Leppard et al. 1996). This resin, however, requires high-hardening temperatures of 60°C, which does not ensure intact rRNA for potential taxonomic staining (see below). Moreover, melamine contains high amounts of nitrogen, which leads to dilution of nitrogen enrichments within organisms.

Other embedding matrices for CARDFISH and NanoSIMS analyses of other types of samples include paraffin (e.g., Jaekel et al. 2013 or Musat et al. 2007) and cryogels (e.g., Wilbanks et al. 2014). Those are, however, not useful for detailed single-cell analyses in marine snow due to the impossibility of section preparations thinner than 5 μm. Additionally, paraffin must be removed after sectioning to allow staining and secondary ion mass spectrometry which increases the risk of material loss due to the high fragility of the marine snow sections dramatically. Cryogels, on the other hand, enable uninterrupted staining but the vacuum resistancy is likely to be suboptimal, and shrinking can be expected, limiting the use for biovolume-corrected enrichment calculations.

As described by Kopf et al. (2015), hard plastic resins are often too dense to allow a variety of staining techniques including CARDFISH. Kopf et al. (2015) and McGlynn et al. (2015) used Technovit, a commercially available acrylic resin. In our tests it turned out, that the also broadly used acrylic resin LR-white (Nussbaumer et al. 2006; Gros and Maurin 2008) showed a high-background fluorescence and was thus not useful for fluorescent stains, such as DAPI.

For our study, we chose a well-established embedding medium mixture based on methacrylate. Key benefits of this medium are that it enables the dissipation of heat during the exothermic polymerization and is characterized by negligible nitrogen and sulfur contents which can affect the significance of enrichment measurements. The medium was optimized for the investigation of human and animal tissue (Burkhardt 1966; Velde et al. 1977) which, like most eumetazoan tissues, contains collagen that acts as a stabilizing matrix during embedding. In contrast, the absence of collagen in marine aggregates leads to disaggregation during the dehydration and infiltration steps. In order to circumvent this limitation, our method employs a pre-embedding step to supplement marine snow with an agarose matrix. Agarose has been used previously as an embedding matrix for marine snow pellets concentrated by centrifugation (Biddanda 1986; Carlough 1994) or for small zooplankton fecal pellets (Gowing and Silver 1983). Agar embedding has been intensively used as for methanotrophic consortia from marine sediments (McGlynn et al. 2015) as well as centrifuged pellets of

bacteria and algae cells (Slaveykova et al. 2009; Kopf et al. 2015). However, as far as we are aware, our method is the first application of an agarose pre-embedding step for preserving structure of undisturbed marine snow. We used low melting-point agarose (liquid state above gelling range of 24–29°C), which facilitates infiltration into typically porous marine aggregates. Furthermore, carbon and hydrogen, the only constituents of agarose, are an advantage when performing isotopic enrichments with nitrogen and sulfur. Combined with the very low nitrogen and sulfur content in the methacrylate resin, dilutions of those elements are reduced. Carbon uptake measurements, on the other hand, require a higher labeling concentration for precise enrichment identification under the same conditions.

The objective of the present study was to develop a working protocol capable of coupling observations of the physical microstructure of marine snow with single-cell uptake rates of organisms within the aggregates. The aggregates, when treated with agarose-methacrylate embedding method, could be consistently sliced to a thickness of 2 μm and exhibited no background fluorescence from the embedding matrix.

Furthermore, we were able to demonstrate the successful staining of methacrylate embedded slices with Alcian Blue for TEP structure, Coomassie Brilliant Blue for proteins, eosin Y for cytoplasm proteins, and DAPI for nucleic acids. Microbes embedded within TEP exudates around algal cells within individual aggregates could be clearly visualized. In contrast, extracellular proteinaceous compounds were not observed in significant amounts, in the aggregates we studied. Moreover, excess Alcian Blue and Coomassie Brilliant Blue dye could be removed without sample loss, reducing any overestimation of TEP and CSP due to precipitation (Passow and Alldredge 1995; Cisternas-Novoa et al. 2015).

We were able to reconstruct the 3D structure of an aggregate portion with its biological (bacterial, algae, eukaryotic cytoplasm) as well as structural (TEP, CSP) compounds. Moreover, we provided a first step toward alternative porosity and 3D fractal dimension calculations using the software BoneJ and its tools originally constructed for trabeculae bone analyses. We have identified further need for a standardized aggregate boundary definition approach.

Thin methacrylate (2 μm) embedded slices had sufficient structural integrity for NanoSIMS analyses under ultra-high vacuum conditions (10^{-10} mbar) with workable ionization efficiencies. Retention of specimen structural integrity is absolutely critical for the calculation of cell volume-corrected elemental enrichments. This was recently demonstrated with pelagic bacteria (Rogge et al. 2017), and is important for calculating the differential uptake of specific elements by heterogeneously sized environmental microorganisms.

We were able to detect and localize prokaryotic uptake of nitrate and sulfate in our sliced marine aggregate preparations. While a dilution of carbon enrichment signals is likely given the C-rich embedding media, even in incubations with

low glucose concentrations (100 nM), a trend toward enrichments was observed visually. The use of higher labeling concentrations in future studies should provide more pronounced results. Moreover, the resin surrounding the organic matter of the aggregate can be used as internal standard to correct abundance calculations and enables precise interpretations.

As an alternative approach for very dense marine snow or marine particles with incorporated terrigenous material, we performed Araldite 502 embeddings. Resulting specimens could be sectioned to a minimum thickness of 40 μm. The applicability for NanoSIMS has already been proven elsewhere (Herrmann et al. 2007; Mueller et al. 2012; Kaiser et al. 2015). Structural staining, however, was not possible with the greater thicknesses, thereby restricting the use of this resin to investigations of nontransparent compounds, such as frustules, pigments, or terrigenous material, and uptake measurements using NanoSIMS.

Finally, we show that our method is also effective for natural aggregates, and we demonstrate the method using aggregates from polar waters off Svalbard. Even though NanoSIMS analyses were not performed on these samples, the reduction of material loss during processing as well as adequate stainability properties could be exemplified. We used the same resin and slice thickness for these samples as for the lab-generated aggregates, and the natural marine snow particles were characterized by identical or similar vacuum resistance specifications as our laboratory generated aggregates.

Future applications for marine snow would benefit from a combination of single cell uptake measurements with identification methods such as rRNA-based catalyzed reporter deposition in situ hybridization (CARDFISH) and related approaches, as demonstrated by several authors for pelagic bacteria (Musat et al. 2008; Krupke et al. 2013; Rogge et al. 2017). This would enable the investigation of physical and metabolic co-location and community structure analyses in marine snow as shown for microbial consortia from marine sediments (McGlynn et al. 2015). In parallel tests, which were not the main focus of this study, we achieved corresponding signals to both positive and negative controls. However, final hybridization optimization and stringency was never achieved and further development would be required. The protocol applied is provided in the Supporting Information Chapter 1 and a similar approach presented by McGlynn et al. (2015).

The method synthesis developed in the present study meets our objective for investigations on marine snow. The pre-embedding procedure maintains 3D structure of the samples and minimizes sample loss primarily because aggregate sections remain embedded in resin during staining process. We demonstrated the ability to identify structural components such as TEP and alkaline amino acids. The identification of prokaryotes and photoautotrophic organisms was also possible using a combination of successful nucleic acid

and eukaryotic cytoplasm staining as wells as Chl *a* autofluorescence of the embedded aggregate slices. Critically, rRNA stays intact during sample preparations with methacrylate resins enabling potential taxonomic staining using CARD-FISH techniques in future applications.

The present protocol provides an opportunity to preserve the structure of marine snow sampled at sea, and investigate microbial activity at the single-cell level within aggregates. We envisage that when our method is applied more broadly to a range of field samples, it will facilitate the development of new insights into aggregate types, sizes and structures, microbial interactions, and aggregate transformation. It will provide input for a new understanding of particle dynamics, as well as for microbial ecology.

We note that in our laboratory-generated aggregates, we also observed the uptake of SO_4, a result which will be of particular interest to follow up in the field, as it points to the potential use of alternative electron acceptors in anoxic microzones within aggregates. The global distribution of aggregate-associated anoxia which increases the global rate of sulfate reduction in the water column was very recently predicted by Bianchi et al. (2018) and our work protocol represents the first tool to investigate those processes in the marine environment. Additionally, slight modifications of the sampling and pre-embedding protocol, such as preaccumulation of aggregates using an elutriation system (Peterson et al. 2005) would enable the investigation of smaller less visible aggregates ($<$ 500 μm). High vacuum tolerance of methacrylate and Araldite resins also allows the use of other modern technologies such as scanning transmission electron microscopy coupled to electron dispersive X-ray analyses, ultimately enabling quantitative element measurements inside organisms, and thus even further possibilities for future applications. A combination of aggregate-related turnover rates with noninvasive optical quantification systems, such as the Underwater Vision Profiler or other systems (Iversen et al. 2010; Picheral et al. 2010; Biard et al. 2016) would ultimately allow us to calculate the contribution of different size classes of aggregates as well as the proportion of involved organisms on regional turnover rates.

We envisage future incorporation into our method of the wide variety of staining protocols already available, enabling further development of application for diverse future investigations.

The cryogel approach presented by Flintrop et al. (2018) focused on structural investigation of marine snow sampled with a Marine Snow Catcher or directly from drifting sediment traps coupled to taxonomic microbial identification using FISH. An overview of major differences and overlaps between plastic resin and the cryogel embedding methods utilized by Flintrop and coworkers is presented in Supporting Information Table S1. In brief, use of a cryogel enables more detailed observations of hydrous compounds due to minimized dehydration, while the resin-embedding process' use

of formaldehyde for chemical fixation, and ethanol or acetone for dehydration, leads to potential loss of diffusible compounds (Grovenor et al. 2006; Kilburn and Clode 2014). If desirable, samples for SIMS analyses of diffusible compounds can be dehydrated using the freeze-approach as described for X-ray microanalyses by Marshall (1980) and more recently for NanoSIMS by Kilburn and Clode (2014). For analyses of nondiffusive compounds, however, acetone dehydration and plastic resin embedding is in fact a widely used method (Herrmann et al. 2007; Clode et al. 2009; Slaveykova et al. 2009; Mueller et al. 2012; Kaiser et al. 2015). Soft and hard plastic embedding resins, particularly methacrylate and Araldite 502, are characterized by ultra-high vacuum-stability, such as minimized shrinking and ablation. Those features, together with the low N and S content, enable cell-volume corrected enrichment calculations with as low as possible isotope dilution effects as reported elsewhere (Rogge et al. 2017). In combination with applicable basic stains (*see* Supporting Information Table S1), detailed elemental uptake investigations of single cells with mechanically undisturbed localization within surrounding organic matrices are possible. Smearing of embedded samples during slicing can go undetected, despite the fact that such smearing significantly reduces their optical resolution and overall effectiveness for analysis. In contrast, any distortion of the sample in a resin can immediately detected because of instantaneous rupture of the slice. Moreover, the alternative embedding matrix Araldite 502, described in this manuscript, enables uptake investigations of marine snow containing very hard compounds as, e.g., terrigenous material. A complementary application of the methods described in this and the manuscript by Flintrop et al. (2018) would enable a wide variety of possible investigations of the microbial ecology and biogeochemical cycling within marine snow as well as effects on the biological carbon pump.

References

Alldredge, A. L., and C. C. Gotschalk. 1988. In situ settling behavior of marine snow. Limnol. Oceanogr. **33**: 339–351. doi:10.4319/lo.1988.33.3.0339

Alldredge, A. L., and M. W. Silver. 1988. Characteristics, dynamics and significance of marine snow. Prog. Oceanogr. **20**: 41–82. doi:10.1016/0079-6611(88)90053-5

Alldredge, A. L., U. Passow, and B. E. Logan. 1993. The abundance and significance of a class of large, transparent organic particles in the ocean. Deep-Sea Res. Part I Oceanogr. Res. Pap. **40**: 1131–1140. doi:10.1016/0967-0637(93)90129-Q

Aylon, Y., and others. 2016. The LATS2 tumor suppressor inhibits SREBP and suppresses hepatic cholesterol accumulation. Genes Dev. **30**: 786–797. doi:10.1101/gad.274167.115

Bako, P., M. Bassiouni, A. Eckhard, I. Gerlinger, C. Frick, H. Löwenheim, and M. Müller. 2015. Methyl methacrylate embedding to study the morphology and immunohistochemistry of adult guinea pig and mouse cochleae. J. Neurosci. Methods **254**: 86–93. doi:10.1016/j.jneumeth.2015.07.017

Becerra, S. C., D. C. Roy, C. J. Sanchez, R. J. Christy, and D. M. Burmeister. 2016. An optimized staining technique for the detection of Gram positive and Gram negative bacteria within tissue. BMC Res. Notes **9**: 216. doi:10.1186/s13104-016-1902-0

Bianchi, D., T. Weber, S. R. Kiko, and C. Deutsch. 2018. Global niche of marine anaerobic metabolisms expanded by particle microenvironments. Nat. Geosci. **65**: 36. doi:10.1038/s41561-018-0081-0

Biard, T., and others. 2016. In situ imaging reveals the biomass of giant protists in the global ocean. Nature **532**: 504–507. doi:10.1038/nature17652

Biddanda, B. A. 1986. Structure and function of marine microbial aggregates. Oceanol. Acta **9**: 209–211.

Burkhardt, R. 1966. Präparative Voraussetzungen zur klinischen histologie des menschlichen Knochenmarkes. Blut **14**: 30–46. doi:10.1007/BF01633163

Busch, K., S. Endres, M. H. Iversen, J. Michels, E.-M. Nöthig, and A. Engel. 2017. Bacterial colonization and vertical distribution of marine gel particles (TEP and CSP) in the Arctic Fram Strait. Front. Mar. Sci. **4**: 1131. doi:10.3389/fmars.2017.00166

Canfield, D. E., F. J. Stewart, B. Thamdrup, L. De Brabandere, T. Dalsgaard, E. F. Delong, N. P. Revsbech, and O. Ulloa. 2010. A cryptic sulfur cycle in oxygen-minimum-zone waters off the Chilean coast. Science **330**: 1375–1378. doi:10.1126/science.1196889

Carlough, L. A. 1994. Origins, structure, and trophic significance of amorphous seston in a blackwater river. Freshw. Biol. **31**: 227–237. doi:10.1111/j.1365-2427.1994.tb00857.x

Carvalho, H. F., and S. R. Taboga. 1996. Fluorescence and confocal laser scanning microscopy imaging of elastic fibers in hematoxylin-eosin stained sections. Histochem. Cell Biol. **106**: 587–592. doi:10.1007/BF02473274

Cisternas-Novoa, C., C. Lee, and A. Engel. 2015. Transparent exopolymer particles (TEP) and Coomassie stainable particles (CSP). Mar. Chem. **175**: 56–71. doi:10.1016/j.marchem.2015.03.009

Clode, P. L., M. R. Kilburn, D. L. Jones, E. A. Stockdale, J. B. Cliff, A. M. Herrmann, and D. V. Murphy. 2009. In situ mapping of nutrient uptake in the rhizosphere using nanoscale secondary ion mass spectrometry. Plant Physiol. **151**: 1751–1757. doi:10.1104/pp.109.141499

Decho, A. W. 1990. Microbial exopolymer secretions in ocean environments: Their role(s) in food webs and marine processes. Oceanogr. Mar. Biol. **28**: 73–153.

DeLong, E. F., D. G. Franks, and A. L. Alldredge. 1993. Phylogenetic diversity of aggregate-attached vs. free-living marine bacterial assemblages. Limnol. Oceanogr. **38**: 924–934. doi:10.4319/lo.1993.38.5.0924

Dörgens, A. L., S. Ahmerkamp, J. Müssig, R. Stocker, M. M. M. Kuypers, A. Khalili, and K. Kindler. 2015. A laboratory model of marine snow. Limnol. Oceanogr.: Methods **13**: 664–671. doi:10.1002/lom3.10056

Doube, M., and others. 2010. BoneJ: Free and extensible bone image analysis in ImageJ. Bone **47**: 1076–1079. doi:10.1016/j.bone.2010.08.023

Fazekas, S., S. Groth, R. G. Webster, and A. Datyner. 1963. Two new staining procedures for quantitative estimation of proteins on electrophoresis strips. Biochim. Biophys. Acta **71**: 377–391. doi:10.1016/0006-3002(63)91092-8

Fazzalari, N. L., and I. H. Parkinson. 1996. Fractal dimension and architecture of trabecular bone. J. Pathol. **178**: 100–105. doi:10.1002/(SICI)1096-9896(199601)178:1<100::AID-PATH429>3.0.CO;2-K

Flintrop, C., A. Rogge, S. Miksch, A. M. Waite, and M. H. Iversen. 2018. Embedding and slicing of intact in situ collected marine snow. Limnol. Oceanogr.: Methods. **16**: 339–355. doi:10.1002/lom3.10251

Fontanez, K. M., J. M. Eppley, T. J. Samo, D. M. Karl, and E. F. DeLong. 2015. Microbial community structure and function on sinking particles in the North Pacific Subtropical Gyre. Front. Microbiol. **6**: 469. doi:10.3389/fmicb.2015.00469

Gormanns, P., S. Reckow, J. C. Poczatek, C. W. Turck, and C. Lechene. 2012. Segmentation of multi-isotope imaging mass spectrometry data for semi-automatic detection of regions of interest. PLoS One **7**: e30576. doi:10.1371/journal.pone.0030576

Gotschalk, C. C., and A. L. Alldredge. 1989. Enhanced primary production and nutrient regeneration within aggregated marine diatoms. Mar. Biol. **103**: 119–129. doi:10.1007/BF00391070

Gowing, M. M., and M. W. Silver. 1983. Origins and microenvironments of bacteria mediating fecal pellet decomposition in the sea. Mar. Biol. **73**: 7–16. doi:10.1007/BF00396280

Gros, O., and L. C. Maurin. 2008. Easy flat embedding of oriented samples in hydrophilic resin (LR White) under controlled atmosphere: Application allowing both nucleic acid hybridizations (CARD-FISH) and ultrastructural observations. Acta Histochem. **110**: 427–431. doi:10.1016/j.acthis.2007.11.001

Grovenor, C. R. M., K. E. Smart, M. R. Kilburn, B. Shore, J. R. Dilworth, B. Martin, C. Hawes, and R. E. M. Rickaby. 2006. Specimen preparation for NanoSIMS analysis of biological materials. Appl. Surf. Sci. **252**: 6917–6924. doi:10.1016/j.apsusc.2006.02.180

Guillard, R. L. L., and J. H. Ryther. 1962. Studies of marine planktonic diatoms. I. Cyclotella nana Hustedt, and Detonula confervacea (cleve) Gran. Can. J. Microbiol. **8**: 229–239. doi:10.1139/m62-029

Heissenberger, A., G. G. Leppard, and G. J. Herndl. 1996a. Relationship between the intracellular integrity and the morphology of the capsular envelope in attached and free-living marine bacteria. Appl. Environ. Microbiol. **62**: 4521–4528.

Heissenberger, A., G. G. Leppard, and G. J. Herndl. 1996b. Ultrastructure of marine snow. II. Microbiological considerations. Mar. Ecol. Prog. Ser. **135**: 299–308. doi:10.3354/meps135299

Herrmann, A. M., P. L. Clode, I. R. Fletcher, N. Nunan, E. A. Stockdale, A. G. O'Donnell, and D. V. Murphy. 2007. A novel method for the study of the biophysical interface in soils using nano-scale secondary ion mass spectrometry. Rapid Commun. Mass Spectrom. **21**: 29–34. doi:10.1002/rcm.2811

Huang, W. M., S. J. Gibson, P. Facer, J. Gu, and J. M. Polak. 1983. Improved section adhesion for immunocytochemistry using high molecular weight polymers of l-lysine as a slide coating. Histochemistry **77**: 275–279. doi:10.1007/BF00506570

Iversen, M. H., N. Nowald, H. Ploug, G. A. Jackson, and G. Fischer. 2010. High resolution profiles of vertical particulate organic matter export off Cape Blanc, Mauritania: Degradation processes and ballasting effects. Deep-Sea Res. Part I Oceanogr. Res. Pap. **57**: 771–784. doi:10.1016/j.dsr.2010.03.007

Jaekel, U., N. Musat, B. Adam, M. Kuypers, O. Grundmann, and F. Musat. 2013. Anaerobic degradation of propane and butane by sulfate-reducing bacteria enriched from marine hydrocarbon cold seeps. ISME J. **7**: 885–895. doi:10.1038/ismej.2012.159

Kaiser, C., M. R. Kilburn, P. L. Clode, L. Fuchslueger, M. Koranda, J. B. Cliff, Z. M. Solaiman, and D. V. Murphy. 2015. Exploring the transfer of recent plant photosynthates to soil microbes: Mycorrhizal pathway vs direct root exudation. New Phytol. **205**: 1537–1551. doi:10.1111/nph.13138

Karner, M., and G. J. Herndl. 1992. Extracellular enzymatic activity and secondary production in free-living and marine-snow-associated bacteria. Mar. Biol. **113**: 341–347. doi:10.1007/BF00347289

Kilburn, M. R., and P. L. Clode. 2014. Elemental and isotopic imaging of biological samples using NanoSIMS. Methods Mol. Biol. **1117**: 733–755. doi:10.1007/978-1-62703-776-1_33

Kimball, S., and P. Mattis, and GIMP Development Team. 1997–2017. GIMP2; [accessed 2018 June 27]. Available from www.gimp.org

Kopf, S. H., S. E. McGlynn, A. Green-Saxena, Y. Guan, D. K. Newman, and V. J. Orphan. 2015. Heavy water and ^{15}N labelling with NanoSIMS analysis reveals growth rate-dependent metabolic heterogeneity in chemostats. Environ. Microbiol. **17**: 2542–2556. doi:10.1111/1462-2920.12752

Kranenburg, C. 1994. The fractal structure of cohesive sediment aggregates. Estuar. Coast. Shelf Sci. **39**: 451–460. doi:10.1016/S0272-7714(06)80002-8

Krupke, A., N. Musat, J. L. Roche, W. Mohr, B. M. Fuchs, R. I. Amann, M. M. M. Kuypers, and R. A. Foster. 2013. In situ identification and N_2 and C fixation rates of uncultivated cyanobacteria populations. Syst. Appl. Microbiol. **36**: 259–271. doi:10.1016/j.syapm.2013.02.002

Leppard, G. G., A. Heissenberger, and G. J. Herndl. 1996. Ultrastructure of marine snow. I. Transmission electron microscopy methodology. Mar. Ecol. Prog. Ser. **135**: 289–298. doi:10.3354/meps135289

Linkert, M., and others. 2010. Metadata matters. J. Cell Biol. **189**: 777–782. doi:10.1083/jcb.201004104

Long, R. A., and F. Azam. 1996. Abundant protein-containing particles in the sea. Aquat. Microb. Ecol. **10**: 213–221. doi:10.3354/ame010213

Lyons, M. M., and F. C. Dobbs. 2012. Differential utilization of carbon substrates by aggregate-associated and water-associated heterotrophic bacterial communities. Hydrobiologia **686**: 181–193. doi:10.1007/s10750-012-1010-7

Maarel, M. J. E. C., W. Sprenger, R. Haanstra, and L. J. Forney. 1999. Detection of methanogenic archaea in seawater particles and the digestive tract of a marine fish species. FEMS Microbiol. Ecol. **173**: 189–194. doi:10.1111/j.1574-6968.1999.tb13501.x

Marshall, A. T. 1980. Freeze-substitution as a preparation technique for biological X-ray microanalysis. Scan. Electron Microsc. 395–408.

Marty, D. G. 1993. Methanogenic bacteria in seawater. Limnol. Oceanogr. **38**: 452–456. doi:10.4319/lo.1993.38.2.0452

McGlynn, S. E., G. L. Chadwick, C. P. Kempes, and V. J. Orphan. 2015. Single cell activity reveals direct electron transfer in methanotrophic consortia. Nature **526**: 531–535. doi:10.1038/nature15512

Moreno-Vivián, C., P. Cabello, M. Martínez-Luque, R. Blasco, and F. Castillo. 1999. Prokaryotic nitrate reduction: Molecular properties and functional distinction among bacterial nitrate reductases. J. Bacteriol. **181**: 6573–6584.

Mueller, C. W., A. Kölbl, C. Hoeschen, F. Hillion, K. Heister, A. M. Herrmann, and I. Kögel-Knabner. 2012. Submicron scale imaging of soil organic matter dynamics using NanoSIMS – from single particles to intact aggregates. Org. Geochem. **42**: 1476–1488. doi:10.1016/j.orggeochem.2011.06.003

Musat, N., O. Giere, A. Gieseke, F. Thiermann, R. Amann, and N. Dubilier. 2007. Molecular and morphological characterization of the association between bacterial endosymbionts and the marine nematode *Astomonema* sp. from the Bahamas. Environ. Microbiol. **9**: 1345–1353. doi:10.1111/j.1462-2920.2006.01232.x

Musat, N., and others. 2008. A single-cell view on the ecophysiology of anaerobic phototrophic bacteria. Proc. Natl. Acad. Sci. USA **105**: 17861–17866. doi:10.1073/pnas.0809329105

Nussbaumer, A. D., C. R. Fisher, and M. Bright. 2006. Horizontal endosymbiont transmission in hydrothermal vent tubeworms. Nature **441**: 345–348. doi:10.1038/nature04793

Paerl, H. W., and J. L. Pinckney. 1996. A mini-review of microbial consortia: Their roles in aquatic production and biogeochemical cycling. Microb. Ecol. **31**: 225–247. doi:10.1007/BF00171569

Passow, U., A. L. Alldredge, and B. E. Logan. 1994. The role of particulate carbohydrate exudates in the flocculation of diatom blooms. Deep-Sea Res. Part I Oceanogr. Res. Pap. **41**: 335–357. doi:10.1016/0967-0637(94)90007-8

Passow, U., and A. L. Alldredge. 1995. A dye-binding assay for the spectrophotometric measurement of transparent exopolymer particles (TEP). Limnol. Oceanogr. **40**: 1326–1335. doi:10.4319/lo.1995.40.7.1326

Passow, U., R. F. Shipe, A. Murray, D. K. Pak, M. A. Brzezinski, and A. L. Alldredge. 2001. The origin of transparent exopolymer particles (TEP) and their role in the sedimentation of particulate matter. Cont. Shelf Res. **21**: 327–346. doi:10.1016/S0278-4343(00)00101-1

Peterson, M. L., S. G. Wakeham, C. Lee, M. A. Askea, and J. C. Miquel. 2005. Novel techniques for collection of sinking particles in the ocean and determining their settling rates. Limnol. Oceanogr.: Methods **3**: 520–532. doi:10.4319/lom.2005.3.520

Phillips, C. J., Z. Smith, T. M. Embley, and J. I. Prosser. 1999. Phylogenetic differences between particle-associated and planktonic ammonia-oxidizing bacteria of the *β* subdivision of the class *Proteobacteria* in the northwestern Mediterranean Sea. Appl. Environ. Microbiol. **65**: 779–786.

Picheral, M., L. Guidi, L. Stemmann, D. M. Karl, G. Iddaoud, and G. Gorsky. 2010. The underwater vision profiler 5. Limnol. Oceanogr.: Methods **8**: 462–473. doi:10.4319/lom.2010.8.462

Ploug, H., M. H. Iversen, and G. Fischer. 2008. Ballast, sinking velocity, and apparent diffusivity within marine snow and zooplankton fecal pellets: Implications for substrate turnover by attached bacteria. Limnol. Oceanogr. **53**: 1878–1886. doi:10.4319/lo.2008.53.5.1878

Polerecky, L., B. Adam, J. Milucka, N. Musat, T. Vagner, and M. M. M. Kuypers. 2012. Look@NanoSIMS–a tool for the analysis of nanoSIMS data in. Environ. Microbiol. **14**: 1009–1023. doi:10.1111/j.1462-2920.2011.02681.x

Rath, J., K. Y. Wu, G. J. Herndl, and E. F. DeLong. 1998. High phylogenetic diversity in a marine-snow-associated bacterial assemblage. Aquat. Microb. Ecol. **14**: 261–269. doi:10.3354/ame014261

Risović, D. 1998. On correlation of fractal dimension of marine particles with depth. J. Colloid Interface Sci. **197**: 391–394. doi:10.1006/jcis.1997.5277

Rogge, A., A. Vogts, M. Voss, K. Jürgens, G. Jost, and M. Labrenz. 2017. Success of chemolithoautotrophic SUP05 and Sulfurimonas GD17 cells in pelagic Baltic Sea redox zones is facilitated by their lifestyles as K- and r-strategists.

Environ. Microbiol. **19**: 2495–2506. doi:10.1111/1462-2920.13783

Schindelin, J., and others. 2012. Fiji: An open-source platform for biological-image analysis. Nat. Methods **9**: 676–682. doi:10.1038/nmeth.2019

Schindelin, J., C. T. Rueden, M. C. Hiner, and K. W. Eliceiri. 2015. The ImageJ ecosystem. Mol. Reprod. Dev. **82**: 518–529. doi:10.1002/mrd.22489

Schmid, B., J. Schindelin, A. Cardona, M. Longair, and M. Heisenberg. 2010. A high-level 3D visualization API for Java and ImageJ. BMC Bioinf. **11**: 274. doi:10.1186/1471-2105-11-274

Schneider, C. A., W. S. Rasband, and K. W. Eliceiri. 2012. NIH image to ImageJ. Nat. Methods **9**: 671–675. doi:10.1038/nmeth.2089

Shanks, A. L., and J. D. Trent. 1979. Marine snow: Microscale nutrient patches. Limnol. Oceanogr. **24**: 850–854. doi:10.4319/lo.1979.24.5.0850

Shiraishi, F., B. Zippel, T. R. Neu, and G. Arp. 2008. In situ detection of bacteria in calcified biofilms using FISH and CARD-FISH. J. Microbiol. Methods **75**: 103–108. doi:10.1016/j.mimet.2008.05.015

Slaveykova, V. I., C. Guignard, T. Eybe, H.-N. Migeon, and L. Hoffmann. 2009. Dynamic NanoSIMS ion imaging of unicellular freshwater algae exposed to copper. Anal. Bioanal. Chem. **393**: 583–589. doi:10.1007/s00216-008-2486-x

Stoderegger, K. E., and G. J. Herndl. 1999. Production of exopolymer particles by marine bacterioplankton under contrasting turbulence conditions. Mar. Ecol. Prog. Ser. **189**: 9–16. doi:10.3354/meps189009

Swan, B. K., and others. 2011. Potential for chemolithoautotrophy among ubiquitous bacteria lineages in the dark ocean. Science **333**: 1296–1300. doi:10.1126/science.1203690

Turley, C. M., and E. D. Stutt. 2000. Depth-related cell-specific bacterial leucine incorporation rates on particles and its biogeochemical significance in the Northwest Mediterranean. Limnol. Oceanogr. **45**: 419–425. doi:10.4319/lo.2000.45.2.0419

Turner, J. T. 2015. Zooplankton fecal pellets, marine snow, phytodetritus and the ocean's biological pump. Prog. Oceanogr. **130**: 205–248. doi:10.1016/j.pocean.2014.08.005

Velde, J. T., R. Burkhardt, K. Kleiverda, L. Leenheers-Binnendijk, and W. Sommerfeld. 1977. Methyl-methacrylate as an embedding medium in histopathology. Histopathology **1**: 319–330. doi:10.1111/j.1365-2559.1977.tb01671.x

Veta, M., J. P. W. Pluim, P. J. van Diest, and M. A. Viergever. 2014. Breast cancer histopathology image analysis: A review. IEEE Trans. Biomed. Eng. **61**: 1400–1411. doi:10.1109/TBME.2014.2303852

Vojvoda, J., D. Lamy, E. Sintes, J. A. L. Garcia, V. Turk, and G. J. Herndl. 2014. Seasonal variation in marine-snow-associated and ambient-water prokaryotic communities in the northern Adriatic Sea. Aquat. Microb. Ecol. **73**: 211–224. doi:10.3354/ame01718

Waheed, A. A., K. S. Rao, and P. D. Gupta. 2000. Mechanism of dye binding in the protein assay using eosin dyes. Anal. Biochem. **287**: 73–79. doi:10.1006/abio.2000.4793

Waite, A. M., K. A. Safi, J. A. Hall, and S. D. Nodder. 2000. Mass sedimentation of picoplankton embedded in organic aggregates. Limnol. Oceanogr. **45**: 87–97. doi:10.4319/lo.2000.45.1.0087

Waite, A. M., Ö. Gustafsson, O. Lindahl, and P. Tiselius. 2005. Linking ecosystem dynamics and biogeochemistry: Sinking fractionation of organic carbon in a Swedish fjord. Limnol. Oceanogr. **50**: 658–671. doi:10.4319/lo.2005.50.2.0658

Wilbanks, E. G., and others. 2014. Microscale sulfur cycling in the phototrophic pink berry consortia of the Sippewissett Salt Marsh. Environ. Microbiol. **16**: 3398–3415. doi:10.1111/1462-2920.12388

Woebken, D., B. M. Fuchs, M. M. M. Kuypers, and R. I. Amann. 2007. Potential interactions of particle-associated anammox bacteria with bacterial and archaeal partners in the Namibian upwelling system. Appl. Environ. Microbiol. **73**: 4648–4657. doi:10.1128/AEM.02774-06

Zoppini, A., A. Puddu, S. Fazi, M. Rosati, and P. Sist. 2005. Extracellular enzyme activity and dynamics of bacterial community in mucilaginous aggregates of the northern Adriatic Sea. Sci. Total Environ. **353**: 270–286. doi:10.1016/j.scitotenv.2005.09.019

Conflict of Interest

None declared.